AIAA SciTech Forum
12-16 January 2026, Orlando, FL
AIAA SCITECH 2026 Forum

10.2514/6.2026-2691

Scaling of Hypersonic Entropy Layers on Blunt-Nosed Wedges

Jaein Lee*, Oliver Schmidt†, and Antonio Sanchez‡
University of California San Diego, La Jolla, CA 92093

A simple method is presented for calculating the structure of entropy layers generated by bow shocks over blunt-nosed wedges in hypersonic flow. The model employs a streamfunction-based framework to track entropy jumps introduced at the bow shock. It is shown that entropy conservation along streamlines, combined with the condition of uniform total enthalpy, determines the transverse profiles of velocity and thermodynamic properties in the downstream parallel-flow region at distances much larger than the wedge radius. A key finding is that the variation of entropy with streamfunction, computed numerically for ideal gas at freestream Mach numbers ranging from $M_\infty = 3$ to $M_\infty = 10$ and wedge half-angles ranging from $\alpha = 0^o$ to $\alpha = 10^o$, identifies a specific nondimensional streamfunction scaled by freestream parameters that collapses the entropy data onto a single quasi-universal curve. The proposed model provides a robust and efficient means of reconstructing the density and velocity fields within the entropy layer for prescribed values of M_∞ and α, eliminating the need for direct CFD simulation and enabling rapid generation of base states for stability analysis and preliminary design.

Nomenclature

α	=	Wedge half-angle
γ	=	Ratio of specific heats
p	=	Static pressure
ρ	=	Density
T	=	Static temperature
U	=	Velocity magnitude
h_t	=	Total enthalpy
s	=	Entropy
Δs	=	Entropy jump across shock
a	=	Nose radius
ψ	=	Streamfunction
$\tilde{\psi}$	=	Nondimensional streamfunction $(\psi/(\rho_{\text{os}} U_{\text{os}} a))$
$F(\tilde{\psi})$	=	Nondimensional function: $(p/p_{\text{os}})^{1/\gamma}(\rho/\rho_{\text{os}})^{-1}$
$F_{norm}(\tilde{\psi})$	=	Normalized entropy function
M_∞	=	Freestream Mach number
ρ_∞	=	Freestream density
U_∞	=	Freestream velocity
p_{os}	=	Post-oblique shock pressure
ρ_{os}	=	Post-oblique shock density
U_{os}	=	Post-oblique shock velocity
c_p	=	Specific heat at constant pressure

*Graduate Research Assistant, Department of Aerospace Engineering, University of California San Diego, 9500 Gilman Drive, La Jolla, CA 92093. AIAA Student Member. jal139@ucsd.edu
†Professor, Department of Aerospace Engineering, University of California San Diego, 9500 Gilman Drive, La Jolla, CA 92093. AIAA Member. oschmidt@ucsd.edu
‡Professor, Department of Aerospace Engineering, University of California San Diego, 9500 Gilman Drive, La Jolla, CA 92093. AIAA Member. alsp@ucsd.edu

I. Introduction

Accurate prediction of laminar-turbulent boundary-layer transition is a critical pacing item in hypersonic vehicle design, as aerothermodynamic heating can rise by an order of magnitude upon transition [1–3]. A common design strategy to mitigate stagnation-point heating is to blunt the vehicle's leading edge. This bluntness, however, introduces profound changes to the post-shock flowfield, creating a complex stability problem that lies outside the domain of classical boundary-layer theory [4].

Blunting generates a detached, highly curved bow shock that imposes non-uniform entropy jumps across streamlines. This inviscid, shock-generated mechanism creates a rotational entropy layer that envelops the body [5]. This layer is defined by strong transverse gradients in temperature and density and persists far downstream. The entropy layer's structure fundamentally alters the boundary layer's stability—a phenomenon studied extensively both experimentally [1, 3, 6, 7] and numerically [2, 8–11]. Key mechanisms include "entropy swallowing," where the boundary layer ingests the entropy layer [12–14], and "transition reversal"—an upstream shift in transition location with increasing bluntness first observed in seminal experiments [1, 15].

Recent high-fidelity numerical studies have clarified the disturbance pathway: the entropy layer supports its own disturbance modes, which can amplify and subsequently feed energy into the viscous boundary layer, triggering the second-mode instability that typically dominates hypersonic transition [16, 17]. This complex, coupled-layer physics, which involves unique receptivity mechanisms [18], demonstrates that an accurate description of the entropy layer's transverse thermodynamic and velocity profiles is a necessary prerequisite for any transition analysis.

A critical gap thus exists in design-oriented tools. High-fidelity Direct Numerical Simulation (DNS) [16, 18] can capture this coupled physics but remains computationally prohibitive for the large parameter sweeps required in preliminary design. Conversely, efficient methods like Linear Stability Theory (LST) or e^N correlations [8, 9] require accurate outer boundary conditions that account for the entropy layer's non-uniform profiles, which are not known a priori.

This paper bridges this gap by developing a simple, physics-based similarity framework for the far-downstream entropy layer structure. For the large values of the Reynolds number characterizing high-speed aerodynamics applications, effects of molecular transport are confined to a thin near-wall boundary layer scaling with the inverse of the Reynolds number, outside of which the flow is nearly inviscid. The resulting simplified description tracks the shock-generated entropy along streamlines, indexed by the streamfunction ψ, and exploits the uniformity of the stagnation enthalpy. The central finding of this work is the discovery of a quasi-universal scaling coordinate. We first demonstrate that conventional scaling using a nondimensional streamfunction based on post-shock conditions, $\tilde{\psi}$, fails to collapse the entropy profiles. We then show that a new coordinate scaled by freestream conditions, $\tilde{\psi}_\infty = \psi/(\rho_\infty U_\infty a)$, surprisingly collapses data from a wide range of Mach numbers (M_∞ = 3.0–10.0) and wedge angles ($\alpha = 0.0^\circ$–10.0°) onto a single quasi-universal curve.

This framework provides a computationally efficient method to reconstruct the far-field density and velocity profiles from only the freestream conditions (M_∞) and wedge half-angle (α). It serves as a simple model, ideal for providing accurate base flows for boundary-layer stability analyses and for enabling rapid, physics-based aerothermodynamic assessments in preliminary vehicle design.

II. Numerical Methodology

A. Geometric Configuration and Computational Mesh

The study considers two-dimensional planar flow over a blunt-nosed wedge, a canonical geometry for hypersonic leading edges. The flowfield, illustrated schematically in Fig. 1, is characterized by a strong, detached bow shock that forms around the circular nose of radius a. Because of the shock's curvature, streamlines passing through the more normal segments of the shock (e.g., the stagnation streamline, entropy s_{ns}) experience a larger entropy increase than those passing through the weaker, more oblique portions (s_{os}). This non-uniform entropy generation creates a high-gradient, inviscid entropy layer (the shaded region in Fig. 1) that persists far downstream, dominating the flow structure.

The inflow boundary was positioned sufficiently upstream to accurately impose freestream conditions and ensure the detached bow shock was fully captured. The lateral boundaries were placed at a sufficient distance to prevent non-physical interactions with the shock. As the present inviscid computation focuses on the entropy layer rather than the viscous boundary layer, the outflow boundary was positioned far downstream at $x = 200a$ to encompass the entire entropy-layer development region [5].

Structured quadrilateral meshes were generated using ANSYS Meshing. Mesh refinement was concentrated near the detached bow shock. To accurately resolve the high-gradient region at the entropy layer's origin, mesh clustering was also applied normal to the wall. While a detailed mesh convergence study is omitted, grid refinement procedures were carried out to confirm that characteristic flow features, such as the shock standoff distance and surface pressure distribution, were grid-independent. A representative grid and the resulting density field are shown in Fig. 2.

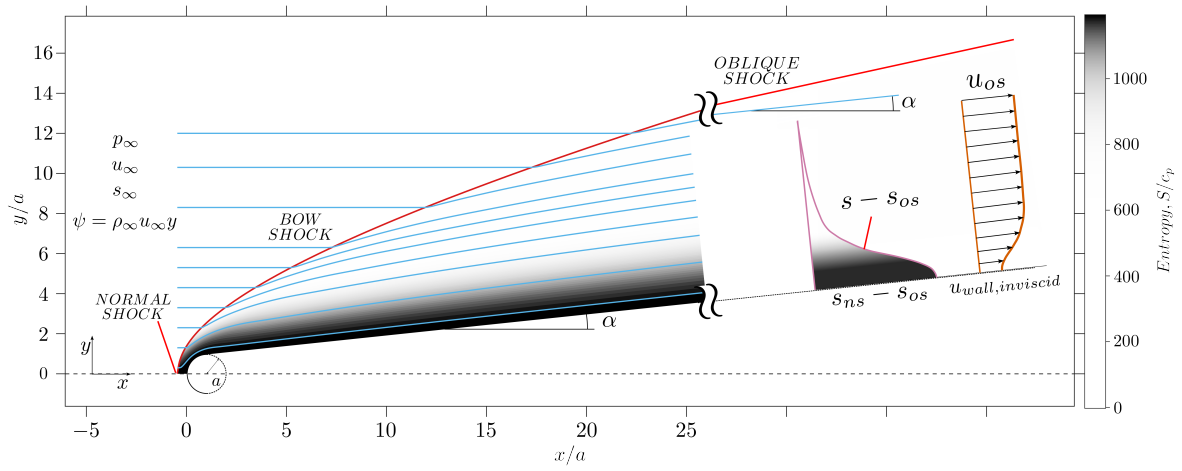

Fig. 1 Schematic of the hypersonic flowfield over a blunt-nosed wedge. The figure illustrates the detached bow shock, the inviscid entropy layer (shaded region, $s > s_{os}$), and the key parameters used in the similarity analysis, including the freestream (u_∞, ψ), post-normal-shock (s_{ns}), and post-oblique-shock (s_{os}, U_{os}) reference states.

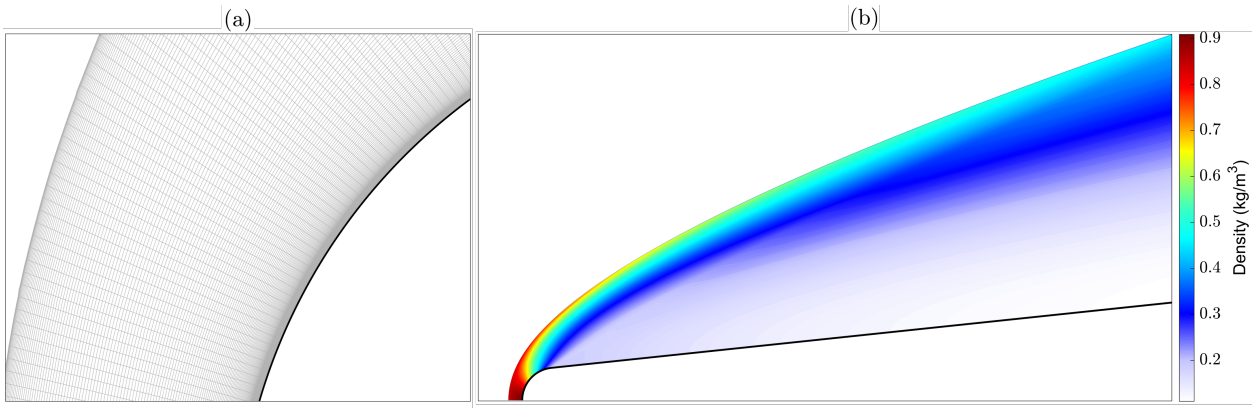

Fig. 2 (a) detail of the structured computational grid, showing the fine mesh resolution near the nose, (b) resulting density contour field (kg/m^3) for the $M = 7.0, \alpha = 7°$, clearly capturing the strong bow shock and flow.

B. Solver Settings and Boundary Conditions

Simulations were performed using the density-based solver in ANSYS Fluent, which is well-suited for hypersonic flows with strong shocks. An implicit formulation was employed to solve the conservative form of the Navier–Stokes equations for mass, momentum, and energy.

Convective terms were discretized using a second-order upwind scheme, with gradients reconstructed via a least-squares cell-based method. Viscous terms employed second-order central differencing. The AUSM flux scheme was selected for its effectiveness in resolving shock and contact discontinuities.

Air was treated as a calorically perfect gas with a constant specific heat ratio of $\gamma = 1.4$, and its viscosity was computed using Sutherland's law. At the surface, a slip-wall boundary condition was enforced along with an adiabatic thermal condition. Steady-state flow was assumed. Turbulence modeling was omitted, as the study focuses on the entropy layer, which is an inviscid feature generated by shock-induced entropy gradients.

C. Parametric Study Matrix

To evaluate the proposed similarity scaling's range of applicability and its robustness, a parametric study was undertaken. The primary independent variables investigated were the freestream Mach number (M_∞) and the wedge half-angle (α). The Mach number was varied from $M_\infty = 3$ to 10, while the wedge half-angle was varied from $\alpha = 0°$ to 10°. These ranges cover typical conditions encountered in hypersonic flight and wind-tunnel experiments where entropy layer effects are significant. All simulations were performed using a constant nose radius of $a = 38.1$ mm. The freestream static pressure and temperature were held at $P_\infty = 7756.56$ Pa and $T_\infty = 174.46$ K, respectively.

III. Theoretical Framework for Similarity Scaling

A. Streamline-Based Entropy Characterization

The thermodynamic state of the entropy layer is path-dependent, determined by the specific shock strength encountered by each streamline. To characterize this variation, we index streamlines by their upstream streamfunction value ψ, defined for planar flow as:

$$\psi(y) = \rho_\infty U_\infty y, \tag{1}$$

where y is the freestream transverse distance from the stagnation line. Outside the thin viscous boundary layer, the flow is inviscid and adiabatic. Consequently, both total enthalpy h_t and entropy s are conserved along streamlines, meaning the local thermodynamic state at any downstream location is a unique function of ψ.

For similarity analysis, it is necessary to define a nondimensional entropy function $F(\tilde{\psi})$. We normalize the local state by the reference post-shock conditions of an equivalent sharp wedge (α, M_∞). For an ideal gas, this function is expressed as:

$$F(\tilde{\psi}) = \exp\left(\frac{s(\psi) - s_{\text{os}}}{\gamma c_v}\right) = \left(\frac{p}{p_{os}}\right)^{1/\gamma} \left(\frac{\rho}{\rho_{os}}\right)^{-1} \tag{2}$$

where s_{os}, p_{os}, and ρ_{os} are the post-oblique-shock reference values. In the far downstream region where pressure equilibrates ($p \approx p_{os}$), this reduces to a direct density mapping $F(\tilde{\psi}) \approx \rho_{os}/\rho(\psi)$.

B. Kinematic Reconstruction via Similarity Mapping

To isolate the self-similar structure of the entropy layer, we introduce a normalized entropy function that scales the post-shock decay relative to the stagnation streamline. The normalized function is defined as:

$$F_{\text{norm}}(\tilde{\psi}) = \frac{F(\tilde{\psi}) - 1}{F(0) - 1} \tag{3}$$

where $F(0)$ represents the maximum entropy state at the stagnation streamline. By inverting Eq. (3) and assuming the profile $F_{\text{norm}}(\tilde{\psi})$ is known, the local thermodynamic state is determined. This analytical reconstruction of the flowfield. Substituting this into the conservation of total enthalpy yields the streamwise velocity profile:

$$\frac{U(\tilde{\psi})}{U_{os}} = \left[1 - \frac{2}{(\gamma - 1)M_{os}^2} \left(F(0) - 1\right) F_{\text{norm}}(\tilde{\psi})\right]^{1/2} \tag{4}$$

With velocity $U(\psi)$ and density $\rho(\psi)$ known from the similarity relation, the final step is to recover the physical wall-normal coordinate n. By integrating the mass conservation relation $dn = (\rho U)^{-1} d\psi$, the physical profile is reconstructed as:

$$n(\psi) = \int_0^\psi \frac{1}{\rho(\hat{\psi})U(\hat{\psi})}\, d\hat{\psi} \tag{5}$$

Equations (4) and (5) constitute a closed-form model, allowing the complete velocity, density, and temperature profiles to be generated in physical coordinates.

IV. Results and Discussion

The primary objective of this investigation is to develop a robust similarity scaling for the thermodynamic and kinematic properties of the hypersonic entropy layer. The analysis begins by evaluating the normalized entropy function, $F_{\text{norm}}(\tilde{\psi})$, defined in Eq. (3), plotted against the post-shock scaled streamfunction $\tilde{\psi} = \psi/(\rho_{\text{os}} U_{\text{os}} a)$. Initial analysis reveals that this simple scaling is insufficient to collapse the data. Figure 3(a) demonstrates this dependency clearly: for a fixed freestream Mach number ($M_\infty = 7.0$), varying the wedge half-angle (α) from 0.0° to 8.0° produces a distinct family of curves. Similarly, Fig. 3(b) shows that for a fixed half-angle ($\alpha = 3.0°$), varying the Mach number from $M_\infty = 3.0$ to 10.0 also results in a significant spread. This confirms that a universal collapse is not possible using only the post-shock reference state.

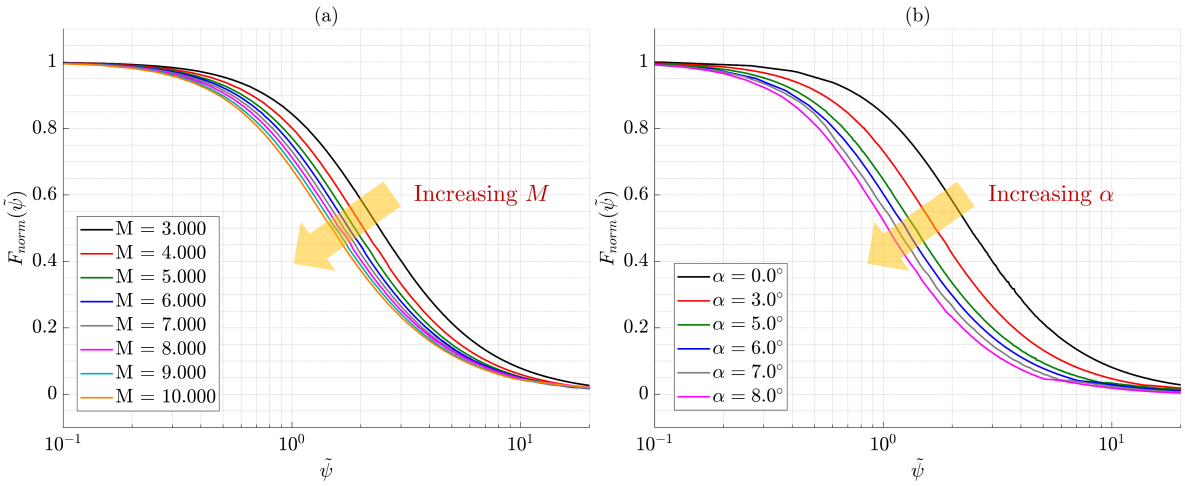

Fig. 3 Analysis of the normalized entropy function, $F_{\text{norm}}(\tilde{\psi})$. (a) Sensitivity to freestream Mach number at a constant wedge half-angle ($\alpha = 3.0°$). (b) Sensitivity to wedge half-angle at a constant Mach number ($M = 7.0$).

A potential path toward a more unified scaling is suggested by hypersonic similarity theory [5]. Figure 4 tests this concept by grouping cases according to the hypersonic similarity parameter $K_{hyp} = M_\infty \alpha$. A close inspection reveals that cases with identical similarity parameters align closely, yet distinct groups do not fully collapse.

A remarkable and effective data collapse is achieved, however, by re-scaling the abscissa. Figure 5 plots the same normalized entropy function against the new nondimensional streamfunction, $\tilde{\psi}_\infty = \psi/(\rho_\infty U_\infty a)$, which is scaled by freestream conditions and reduces to the ratio of the distance to the centerline to the nose radius. Plotted in this manner, the data from all simulated cases—spanning a wide range of freestream Mach numbers ($M_\infty = 5.0$ to 10.0) and wedge half-angles ($\alpha = 0.0°$ to 9.0°)—converge onto a single, quasi-universal curve. This somewhat surprising collapse validates $\tilde{\psi}_\infty$ as the proper similarity coordinate for the entropy layer's thermodynamic structure.

This universal thermodynamic profile provides the necessary closure for the kinematic reconstruction framework derived in Sec. III. By substituting the collapsed entropy profile into Eq. (4), the local velocity U is determined analytically. Subsequently, the physical wall-normal coordinate n is recovered via the integral transformation in Eq. (5). Together, these relations form a complete predictive model that reconstructs the entire velocity profile $U(n/a)$ based solely on the universal entropy curve.

The utility of this thermodynamic scaling extends directly to the kinematic field. By establishing a universal curve for the entropy function, the velocity profile far downstream can be analytically reconstructed using the energy conservation relation (Eq. (4)) without requiring a full CFD solution for that downstream region. Figure 6 provides a direct validation of this predictive capability. It compares the velocity profiles from the full CFD simulations (symbols) with the profiles predicted by the scaling model (lines) at a far-downstream location of $x/a = 200$. The model demonstrates excellent agreement across all cases, accurately capturing the velocity deficit within the entropy layer. The right panel, a zoomed-in view, confirms the model's precision even in the high-gradient region near the wall. This result underscores the model's power as a computationally efficient tool for accurately predicting the far-field aerothermodynamic environment.

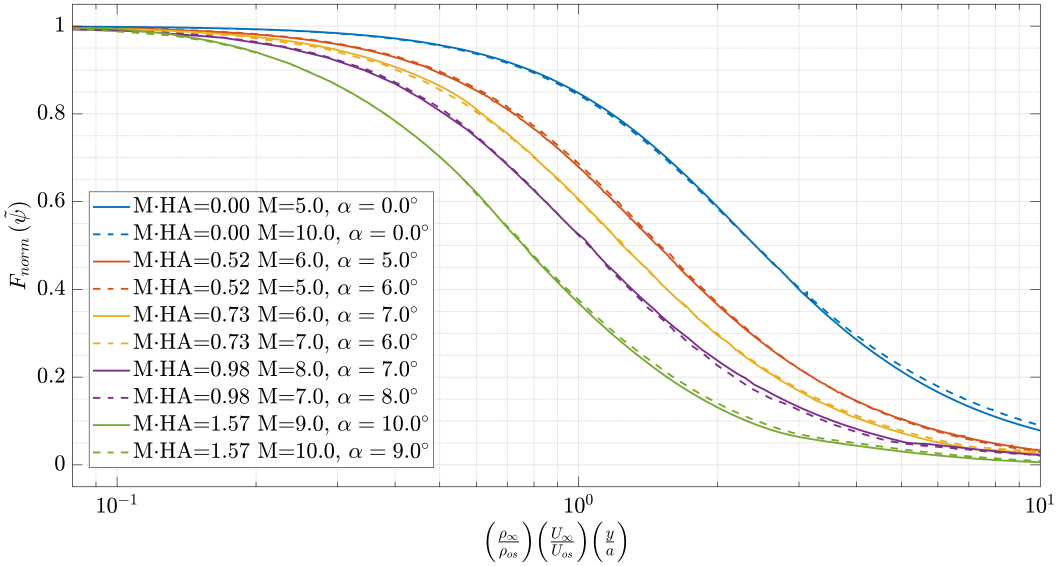

Fig. 4 Grouping of entropy profiles by the hypersonic similarity parameter 'M-HA'. Cases with the same 'M-HA' value but different (M_∞, α) pairs (e.g., solid and dashed lines of the same color) show close alignment, but different 'M-HA' groups do not collapse.

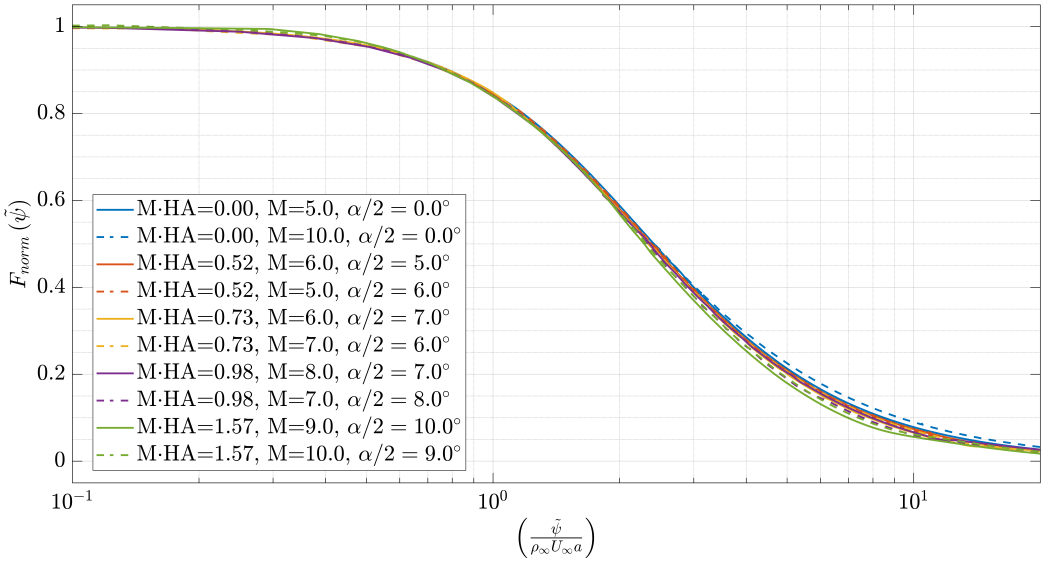

Fig. 5 Collapse of the normalized entropy function for all cases onto a quasi-universal curve. The collapse is achieved by plotting against the nondimensional streamfunction scaled by freestream conditions, $\tilde{\psi}_\infty = \psi/(\rho_\infty U_\infty a)$.

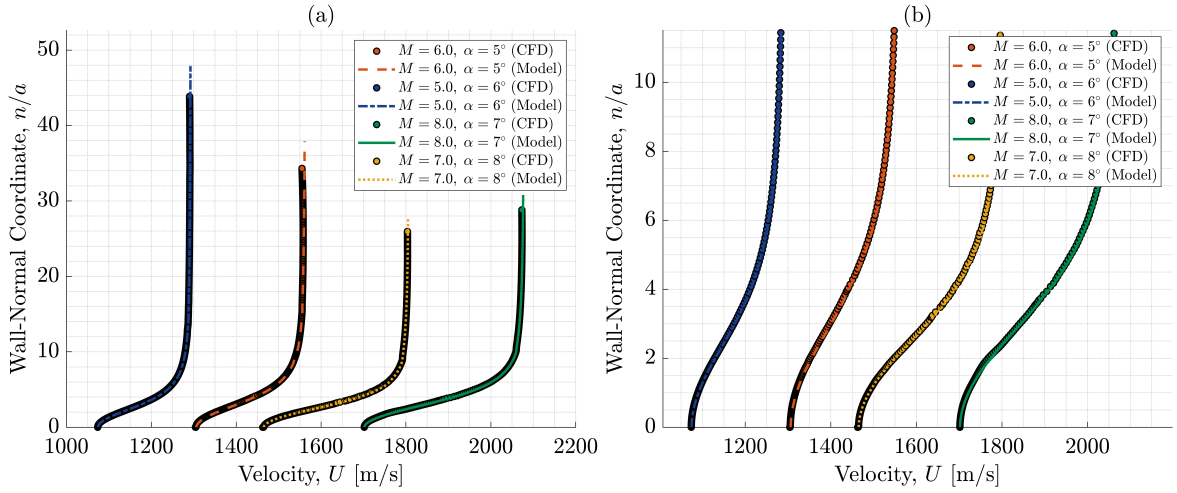

Fig. 6 Validation of the scaling model's predictive capability for velocity profiles at a far-downstream location ($x/a = 200$). CFD results (symbols) are compared with the analytical model (lines) for various M_∞ and α. The right panel provides a zoomed-in view near the wall.

V. Conclusion

A similarity scaling framework for the entropy layer on hypersonic blunt-nosed wedges has been developed across a wide range of freestream Mach numbers ($M_\infty = 3.0$–10.0) and wedge half-angles ($\alpha = 0.0°$–$10.0°$). This investigation first demonstrated that conventional scaling approaches, which rely on post-oblique-shock reference quantities for the streamfunction ($\tilde{\psi}$), are insufficient to collapse the normalized entropy profiles, as the data retains a clear dependency on both M_∞ and α. The core achievement of this work is the discovery and validation of a new, quasi-universal scaling coordinate, $\tilde{\psi}_\infty = \psi/(\rho_\infty U_\infty a)$, which, being scaled by freestream conditions, reduces to the ratio of the distance to the centerline to the nose radius. When the normalized entropy function, F_{norm}, is plotted against $\tilde{\psi}_\infty$, data from all simulated cases converge onto a quasi universal curve. This successful collapse reveals a fundamental self-similarity in the entropy layer's thermodynamic structure. This quasi universal curve, in conjunction with energy conservation relations, enables the accurate and analytical reconstruction of the far-downstream velocity field, a result validated against the CFD data. This work thus provides an efficient, physics-based engineering tool, with the important caveat that the scaling is validated for the far-field ($x/a \gg 1$) where the flow has achieved a self-similar state.

References

[1] Stetson, K. F., "Nosetip Bluntness Effects on Cone Frustum Boundary Layer Transition in Hypersonic Flow," *16th Fluid and Plasmadynamics Conference*, AIAA, 1983, pp. Paper No. AIAA 1983–1763.

[2] Reshotko, E., and Khan, M. M. S., "Stability of the Laminar Boundary Layer on a Blunted Plate in Supersonic Flow," *Laminar-Turbulent Transition*, edited by W. S. Saric, Pergamon Press, 1980, pp. 377–391. Presented at the IUTAM Symposium, Nov. 1979.

[3] Potter, J. L., "Boundary Layer Transition on Supersonic Cones in an Aerobalistic Range," *AIAA Journal*, Vol. 13, No. 3, 1975, pp. 270–277. https://doi.org/10.2514/3.49692.

[4] Hayes, W. D., and Probstein, R. F., *Hypersonic Flow Theory*, Academic Press, New York, 1966.

[5] Anderson, J. D. J., *Hypersonic and High Temperature Gas Dynamics*, 3rd ed., American Institute of Aeronautics and Astronautics, Reston, VA, 2006. https://doi.org/10.2514/4.866825.

[6] Stetson, K. F., Thompson, E. R., Donaldson, J. C., and Siler, L. G., "Laminar Boundary Layer Stability Experiments on a Cone at Mach 8. I—Sharp Cone," *16th Fluid and Plasmadynamics Conference*, AIAA, 1983, pp. Paper No. AIAA 1983–1761.

[7] Huang, R., Cheng, J., Chen, J., Yuan, X., and Wu, J., "Experimental study of bluntness effects on hypersonic boundary-layer transition over a slender cone using surface mounted pressure sensors," *Advances in Aerodynamics*, Vol. 4, No. 1, 2022, p. 35. https://doi.org/10.1186/s42774-022-00128-z.

[8] Malik, M. R., Spall, R. E., and Chang, C.-L., "Effect of Nose Bluntness on Boundary Layer Stability and Transition," *28th Aerospace Sciences Meeting*, AIAA, 1990, pp. Paper No. AIAA 1990–0112.

[9] Li, X., Fu, D., and Ma, Y., "Direct Numerical Simulation of Hypersonic Boundary Layer Transition over a Blunt Cone," *AIAA Journal*, Vol. 46, No. 11, 2008, pp. 2899–2913. https://doi.org/10.2514/1.37356.

[10] Zhong, X., and Ma, Y., "Boundary-layer receptivity of Mach 7.99 flow over a blunt cone to free-stream acoustic waves," *Journal of Fluid Mechanics*, Vol. 556, 2006, pp. 55–100. https://doi.org/10.1017/S002211200600930X.

[11] Zhou, J., and Cao, W., "Effects of entropy layer on the boundary layer over hypersonic blunt cones considering entropy swallowing," *Physics of Fluids*, Vol. 33, No. 7, 2021, p. 076102. https://doi.org/10.1063/5.0055393.

[12] Krause, E., and Zakkay, V., "Boundary conditions at the outer edge of the boundary layer on blunted conical bodies," *AIAA Journal*, Vol. 1, No. 7, 1963, pp. 1671–1672. https://doi.org/10.2514/3.1899.

[13] Rushton, G. H., and Stetson, K. F., "Shock tunnel investigation of boundary-layer transition at $M = 5.5$," *AIAA Journal*, Vol. 5, No. 5, 1967, pp. 899–906. https://doi.org/10.2514/3.4108.

[14] Marineau, E. C., Moraru, G. C., Lewis, D. R., Norris, J. D., and Lafferty, J. F., "Mach 10 Boundary Layer Transition Experiments on Sharp and Blunted Cones," Tech. Rep. AIAA Paper 2014-3108, Naval Surface Warfare Center Dahlgren Division, Atlanta, GA, June 2014. https://doi.org/10.2514/6.2014-3108, presented at the AIAA Aviation and Aeronautics Forum and Exposition (AVIATION 2014).

[15] Softley, E. J., Graber, B. C., and Zempel, R. E., "Experimental Observation of Transition of the Hypersonic Boundary Layer," *AIAA Journal*, Vol. 7, No. 2, 1969, pp. 257–263. https://doi.org/10.2514/3.5034.

[16] Wan, B., Su, C., and Chen, J., "Receptivity of a Hypersonic Blunt Cone: Role of Disturbances in Entropy Layer," *AIAA Journal*, Vol. 58, No. 9, 2020, pp. 4047–4054. https://doi.org/10.2514/1.J058978.

[17] Goparaju, H., Unnikrishnan, S., and Gaitonde, D. V., "Effects of Nose Bluntness on Hypersonic Boundary-Layer Receptivity and Stability," *Journal of Spacecraft and Rockets*, Vol. 58, No. 3, 2021, pp. 668–684. https://doi.org/10.2514/1.A34904.

[18] Zhong, X., and Wang, X., "Direct Numerical Simulation on the Receptivity, Instability, and Transition of Hypersonic Boundary Layers," *Annual Review of Fluid Mechanics*, Vol. 44, No. 1, 2012, pp. 527–561. https://doi.org/10.1146/annurev-fluid-120710-101208.